LOCAL HEAT TRANSFER ON A FINITE WIDTH SURFACE WITH LAMINAR BOUNDARY LAYER FLOW

M. E. Taliaferro*, M. Angelino*, F. Gori**, R. J. Goldstein*

*University of Minnesota, 111 Church Street SE, Minneapolis MN, 55455
**University of Rome "Tor Vergata", Via del Politecnico 1, 00133 Roma, Italy

ABSTRACT

The effect of a lateral discontinuity in the thermal boundary conditions in two dimensional laminar flow on a flat plate, is investigated by numerical and analytical modeling. When the thermal and momentum boundary layers start at the same location, the resulting self-similar two dimensional boundary layer equations were solved numerically. For an unheated starting length, three dimensional numerical simulations were required. For both the three and two dimensional thermal simulations, a Blasius velocity field was assumed. It is found that all the Nusselt numbers collapse to a single curve when graphed as a function of a spanwise similarity variable. Simple correlations for the local Nusselt number on a rectangular flat plate are presented for a variety of boundary conditions.

Keywords: *Laminar, Nusselt number, finite lateral span*

INTRODUCTION

Cooling of electronic components is an important design consideration for digital systems. Many of these have discrete rectangular heat sources that are cooled in a channel, but modeling both the fluid flow and the conduction in the substrate can be a prohibitively expensive task. Many studies seek to simplify this by presenting correlations for the heat transfer coefficient so the modeling of the fluid can be ignored. This allows designers to model only the conduction in the substrate with convective boundary conditions.

Several studies have investigated the effect of finite surface on the heat transfer coefficient from flat plates. Baker conducted one of the first studies of small heaters [1], and noted that the average heat transfer coefficient could be more than an order of magnitude more than predicted by the canonical two dimensional flat plate correlations. Other studies have reported heat transfer coefficient correlations that also take into account the conductivity of the substrate [2; 3]. Bhowmik [4] recently published a short review of the subject.

However, to accurately predict the temperature of the electronic device, knowledge of the local Nusselt number is required. Ortega and Ramanathan [5] propose using point source solutions for the energy equation assuming bulk flow, and then superposing them to form a general equation for the convection losses from rectangles and line sources. Instead of assuming constant heat flux [5], Yovanovich and Teertstra [6] report the average *Nu* for an isothermal plate by averaging the solutions for the diffusive limit and convective limit (i.e. for low and high *Re*). This paper presents several correlations that describe the lateral variation of the *Nu* for use with discrete rectangular heat sources that are flush with the substrate surface for several types of boundary conditions. These correlations can then be used a basis for modeling the more complicated problem of conjugated heat transfer between the air flow and the substrate.

Governing Equations

For steady and incompressible flow with constant properties, the energy equation from Kays, Crawford and Weigand [7] is

$$\vec{V} \cdot \nabla T = \alpha \nabla^2 T \tag{1}$$

A sketch of the problem domain appears in figure 1. If the

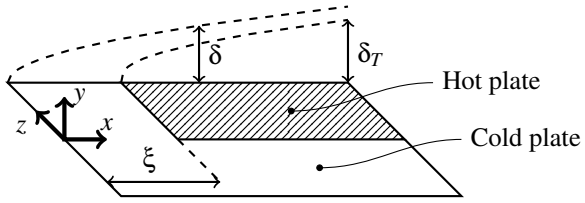

Figure 1. Problem domain showing orientation and boundary layer development

streamwise conduction is assumed negligible, then equation 1 can be simplified as followed. For two dimensional flow, $w = 0$, so

$$u\frac{\partial T}{\partial x} + v\frac{\partial T}{\partial y} = \alpha\left(\frac{\partial^2 T}{\partial y^2} + \frac{\partial^2 T}{\partial z^2}\right) \tag{2}$$

If the momentum and thermal boundary layers start at the same position ($\xi = 0$) and the following two variables are defined, as done by Hauptmann and Rotem [8],

$$\eta = y\sqrt{\frac{U_\infty}{\nu x}}, \quad \zeta = z\sqrt{\frac{U_\infty}{\nu x}} \tag{3}$$

and f is the solution to the Blasius equation, equation 2 can be reduced to the following two dimensional equation

$$-\frac{Pr}{2}\left(\zeta f'\frac{\partial\theta}{\partial\zeta}+f\frac{\partial\theta}{\partial\eta}\right)=\frac{\partial^2\theta}{\partial\eta^2}+\frac{\partial^2\theta}{\partial\zeta^2} \tag{4}$$

Four types of boundary conditions were solved for, and are summarized in table 1.

Table 1. Boundary conditions

Case	Heated Surface	Undeated Surface
1	Isothermal	Isothermal
2	Isothermal	Adiabatic
3	Isoflux	Isothermal
4	Isoflux	Adiabatic

RESULTS

Very close to the surface of the plate, conduction is the main mode of thermal transport, and the spanwise changes in the Nu can be attributed to the discontinuity in the z direction at the lateral edge of the plate. The height of the domain, Δ_c, is assumed to only change in the streamwise direction. Therefore, near the surface of the plate, the temperature distribution is expected to be well represented by the temperature field of the analogous conduction problems shown in figure 2 and figure 3. Under these conditions, $u=v=0$, simplifying equation 2 to Laplace's equation in two dimensions.

$$0=\frac{\partial^2 T}{\partial y^2}+\frac{\partial^2 T}{\partial z^2} \tag{5}$$

Conduction Solution

In this section the conduction solution for the different boundary conditions will be presented. Case 1 and case 4 can readily be solved using Fourier series, but the analytical solution for case 2 and case 3 are difficult to formulate, so approximate solutions are presented. The conduction domain, as shown in figure 2 and figure 3 is a $y-z$ plane taken out the region described in figure 1. Integrations were performed with Wolfram|Alpha.

Case 1 The eigenfunctions for the boundary conditions for figure 2, are given by Ozisik [9] as

$$\frac{\theta_{1,\lambda}(y,z)}{\theta_s}=A_{\lambda,1}\exp(-\lambda_{n,T}z)\sin(\lambda_{n,T}y),\quad z>0 \tag{6a}$$
$$\frac{\theta_{2,\lambda}(y,z)}{\theta_s}=A_{\lambda,2}\exp(\lambda_{n,T}z)\sin(\lambda_{n,T}y),\quad z<0 \tag{6b}$$

where θ is temperature relative to the free stream temperature. The eigenvalues are $(\lambda_{n,T})$ given by

$$\lambda_{n,T}=\frac{n\pi}{\Delta_c},\quad n=1,2,3,... \tag{7}$$

Noting that as $z\to\infty$ the solution tends towards the one dimensional linear solution, as $z\to-\infty$ the solution tends towards zero, and enforcing temperature and lateral flux continuity at the interface results in the solution shown in equation 8.

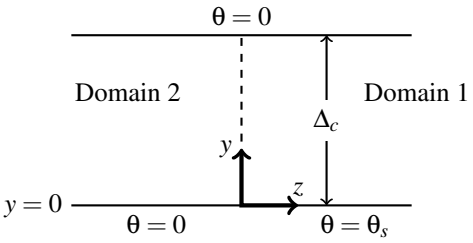

Figure 2. Sketch of domain for conduction problem for boundary condition case 1

$$\frac{\theta_1(y,z)}{\theta_s}=1-\frac{y}{\Delta_c}-\sum_{n=1}^{\infty}\frac{\exp(-\lambda_{n,T}z)}{n\pi}\sin(\lambda_{n,T}y),\quad z>0 \tag{8a}$$
$$\frac{\theta_2(y,z)}{\theta_s}=\sum_{n=1}^{\infty}\frac{\exp(\lambda_{n,T}z)}{n\pi}\sin(\lambda_{n,T}y),\quad z<0 \tag{8b}$$

The quantity of interest is the flux from the surface, which is proportional to the temperature gradient evaluated at the surface. For domain 1, the temperature gradient at $y=0$ is

$$\frac{1}{\theta_s}\frac{\partial\theta_1}{\partial y}\bigg|_0=-\frac{1}{\Delta_c}\left[1+\frac{1}{\exp\left(n\pi\frac{z}{\Delta_c}\right)-1}\right] \tag{9}$$

Case 4 Similar to the solution procedure presented for case 1, a solution can be constructed for the conduction problem shown in figure 3.

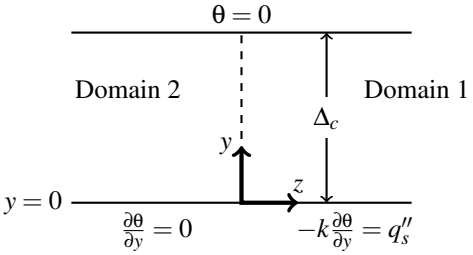

Figure 3. Sketch of domain for conduction problem for boundary condition case 4

The eigenfunctions for the boundary conditions for figure 3, are given by Ozisik [9] as

$$\theta_{1,\lambda}(y,z)=B_{\lambda,1}\exp(-\lambda_{n,F}z)\cos(\lambda_{n,F}y),\quad z>0 \tag{10a}$$
$$\theta_{2,\lambda}(y,z)=B_{\lambda,2}\exp(\lambda_{n,F}z)\cos(\lambda_{n,F}y),\quad z<0 \tag{10b}$$

where the eigenvalues are $(\lambda_{n,F})$ given by

$$\lambda_{n,F}=\frac{(2n+1)\pi}{2\Delta_c},\quad n=0,1,2,... \tag{11}$$

With these eigenvalues and eigenfunctions, the full solution for case 2 is

$$\frac{k}{q_s''\Delta_c}\theta_1(y,z) = 1 - \frac{y}{\Delta_c} - \frac{4}{\pi^2}\sum_{n=0}^{\infty}\frac{\exp(-\lambda_{n,F}z)}{(2n+1)^2}\cos(\lambda_{n,F}y), \quad z>0 \quad (12a)$$

$$\frac{k}{q_s''\Delta_c}\theta_2(y,z) = \frac{4}{\pi^2}\frac{q_s''\Delta_c}{k}\sum_{n=0}^{\infty}\frac{\exp(\lambda_{n,F}z)}{(2n+1)^2}\cos(\lambda_{n,F}y), \quad z<0 \quad (12b)$$

Note that equation 12 equals $^1/_2$ when $z=0$ and the temperature evaluated at $y=0$ is an odd function shifted up by $^1/_2$.

Cases 2 and 3 For cases 2 and 3 a closed form analytical solution is difficult to formulate, but a reasonably accurate approximate solution is presented. To approximate the analytical solution, the result was assumed to be a linear sum of the eigenfunctions in equation 6 and equation 10. The linear sum of eigenfunctions were fitted to a numerical solution found with OpenFOAM with the same boundary conditions to find the coefficients A_λ and B_λ. The linear best fit gave an approximate solution for case 2 as

$$\frac{\theta_1(y,z)}{\theta_s} = 1 - \frac{y}{\Delta_c} - 0.162\sum_{n=1}^{\infty}\frac{\exp(-\lambda_{n,T}z)}{n^{1.4525}}\sin(\lambda_{n,T}y), \quad z>0 \quad (13a)$$

$$\frac{\theta_2(y,z)}{\theta_s} = 0.492\sum_{n=0}^{\infty}\frac{\exp(\lambda_{n,F}z)}{(2n+1)^{1.5706}}\cos(\lambda_{n,F}y), \quad z<0 \quad (13b)$$

The temperature gradient evaluated at the wall for the heated section

$$\frac{1}{\theta_s}\left.\frac{\partial\theta}{\partial y}\right|_0 = -\frac{1}{\Delta_c}\left[1 + 0.509\sum_{n=1}^{\infty}\frac{\exp\left(-n\pi\frac{z}{\Delta_c}\right)}{n^{0.4525}}\right] \quad (14)$$

For case 3, the temperature is approximated by

$$\frac{k}{q_s''\Delta_c}\theta_1(y,z) = 1 - \frac{y}{\Delta_c} - 0.492\sum_{n=0}^{\infty}\frac{\exp(-\lambda_{n,F}z)}{(2n+1)^{1.5706}}\cos(\lambda_{n,F}y), \quad z>0 \quad (15a)$$

$$\frac{k}{q_s''\Delta_c}\theta_2(y,z) = 0.162\sum_{n=1}^{\infty}\frac{\exp(\lambda_{n,T}z)}{n^{1.4525}}\sin(\lambda_{n,T}y), \quad z<0 \quad (15b)$$

Due to the approximations used in formulating equation 13 and equation 15, the temperatures do not match at $z=0$. The difference in the nondimensional temperature is about 0.02. The error for the lateral flux at the interface was a little more difficult to quantify because of the Gibbs phenomena near the discontinuity on the wall.

Convection Correlations

The conduction solution outlined above can be extended to model the *Nu* for a flat plate with a laminar flow boundary layer. To match the *Nu* as $z\to\infty$, Δ_c is taken to be the conduction thickness of the thermal boundary layer far from the lateral edge of the plate.

$$\Delta_c = \frac{x}{Nu_{2d}} \quad (16)$$

where Nu_{2d} is the *Nu* far from the edge at the same x location. The value for Δ_c is readily available using *Nu* correlations for the two dimensional flow over a flat plate in terms of Re, Pr, and the unheated starting length ξ.

Inspecting the gradients at the wall from the conduction solution, it is apparent that z appears with Δ_c as a ratio. If a new parameter, ζ^*, is defined as

$$\zeta^* = \frac{z}{\Delta_c} = \frac{z}{x}Nu_{2d} = -\zeta\left.\frac{\partial T}{\partial\eta}\right|_{\eta=0,\zeta\to\infty} \quad (17)$$

then the conduction solutions and ζ^* can be combined to find *Nu* over the whole plate. For case 1, using equations 17 and 9, *Nu* is equivalent to

$$\frac{Nu}{Nu_{2d}} = 1 + \frac{1}{\exp(\pi\zeta^*) - 1} \quad (18)$$

For case 4, *Nu* is equivalent to

$$\frac{Nu}{Nu_{2d}} = \frac{1}{1 - \frac{4}{\pi^2}\exp\left(-\frac{\pi}{2}\zeta^*\right)\sum_{n=0}^{\infty}\frac{\exp(-n\pi\zeta^*)}{(2n+1)^2}} \quad (19)$$

Note that Nu/Nu_{2d}i s the reciprocal of the nondimensional temperature $\theta k/q_s''\Delta_c$ evaluated at $y=0$. For case 2, *Nu* is approximately

$$\frac{Nu}{Nu_{2d}} = 1 + 0.509\sum_{n=1}^{\infty}\frac{\exp(-n\pi\zeta^*)}{n^{0.4525}} \quad (20)$$

For case 3, *Nu* is approximately

$$\frac{Nu}{Nu_{2d}} = \frac{1}{1 - 0.614\exp\left(-\frac{\pi}{2}\zeta^*\right)\sum_{n=0}^{\infty}\frac{\exp(-n\pi\zeta^*)}{(2n+1)^{1.5706}}} \quad (21)$$

Equations 18 through 20 are compared with the two and three dimensional numerical simulations in figures 9 through 11, as discussed below.

Since equation 21 does not capture the behavior of the *Nu* as $\zeta^*\to 0$, and 20 is slow to converge, alternate correlations will be constructed. Following the method outlined by [10], an average will be taken that captures the behavior as $\zeta^*\to 0$ and $\zeta^*\to\infty$. The two dimensional data modeled by equation 4 will be used to fit the correlation. As seen in figure 10 and figure 11, as $\zeta^*\to 0$, then $\frac{Nu}{Nu_{2d}}\propto\zeta^{*^{-1/2}}$, so the correlation is

$$\frac{Nu}{Nu_{2d}} = \left[\left(c\zeta^{*^{-1/2}}\right)^m + 1\right]^{1/m} \quad (22)$$

Fitting this equation using a least squares regression for case 3 results in $m = 4.324$ and $c = 0.8495$ with a maximum relative error of 4.5 %. Fitting equation 22 for case 2 results in $m = 3.709$ and $c = 0.6149$ for a maximum relative error of 2.5 %.

Computational Details

For the cases with no unheated starting lengths, the passive scalar θ in equation 4 was numerically solved using the solver scalarTransportFoam from the open-source code OpenFOAM. The velocity field was initialized with the Blasius solution. The size of the domain was $-20 < \eta < 20$ and $0 < \zeta < 20$. The grid is made of 2048×1024 cells with a minimum size at $\eta = \zeta = 0$ of about $\left(4 \times 10^{-4}\eta\right) \times \left(4 \times 10^{-4}\zeta\right)$. The boundary conditions for the wall are specified according the particular case being modeled, zero temperature at the top and left boundaries, and zero gradient at the right boundary.

For the cases with unheated starting lengths, the passive scalar T in equation 1 was numerically solved using the solver scalarTransportFoam from the open-source code OpenFOAM. The 3D geometry consists of a rectangular box with $-0.02L < (x-\xi) < L$, $0 < y < 0.3L$, and $-0.1L < z < 0.1L$, where L is the length of the heated plate. The distance from the leading edge is denoted by x, while ξ is the unheated starting length, so that the heated plate is the part of the wall limited by $(x-\xi) > 0$ and $z > 0$. Two unheated starting lengths were studied, corresponding to $Re_\xi = 5 \times 10^3$ and 5×10^4. The grid is made of $192 \times 64 \times 256$ cells with a minimum size at $x = \xi$ and $z = 0$ of about $(10^{-4}L) \times (10^{-4}L) \times (3 \times 10^{-5}L)$. Three different Prandtl numbers were used: 0.7, 2.28, and 6. The boundary conditions for the wall are specified according the particular case being modeled, adiabatic at the top, the outlet, and the left and right boundaries, and zero temperature at the inlet.

Grid independence was checked by comparing the *Nu* profiles on the heated plate obtained with three different meshes: the mesh described in the preceding paragraph, used for all the 3D simulations of the present study; a finer mesh with same number of cells but halved domain in the y and z direction; and a coarser mesh with same number of cells but doubled domain in the y and z direction. The results for case 1 are shown in figure 4, together with expected result from equation 18. It is clear that the cells closer to the lateral edge of the heated plate diverge from the theoretical solution. This is expected, given that the gradient tends to infinity as $\zeta \to 0$ as predicted by equation 18, and the progressively finer meshes in figure 4 seem to imply the same phenomena. However, there can only be a finite amount of cells in that region, so refining the mesh just shifts the problem closer to the lateral edge. Therefore, there is no possible refinement of the cartesian grid can capture the infinite gradient at the lateral discontinuity. The choice of the grid was then determined by considerations of the domain size, which had to be large enough for the boundaries to be far from the effects of the plate.

DISCUSSION OF RESULTS

Figure 5 through figure 8 show the nondimensional temperature contours of the two-dimensional solution of equation 4. These figures show that the depth of the effect into the temperature field from the edge is similar in magnitude to the two dimensional thermal boundary layer thickness. The bulge in figure 5 and figure 7 is caused by the zero temperature boundary condition at the surface.

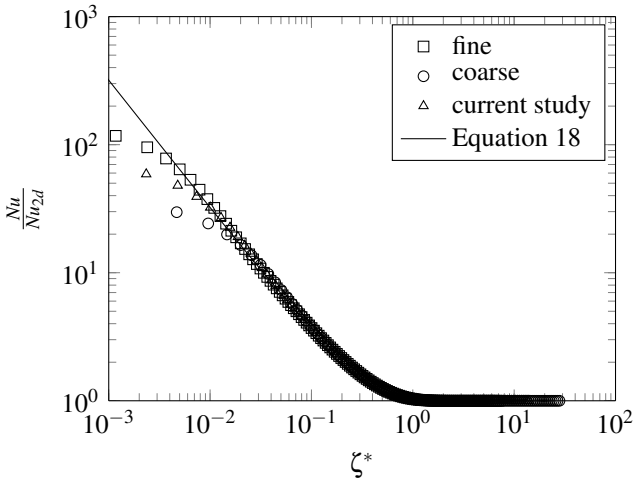

Figure 4. Grid independence study for case 1

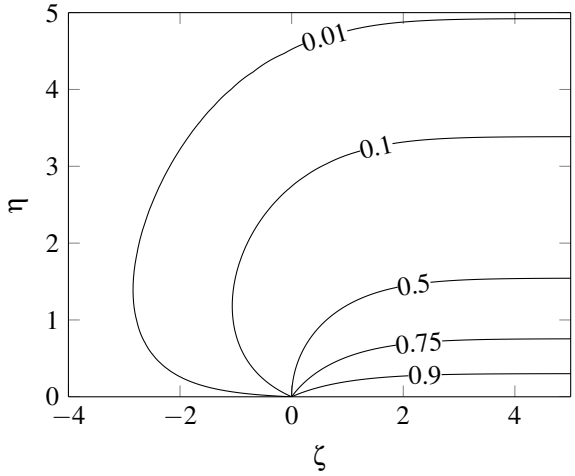

Figure 5. Nondimensional temperature (θ/θ_s) contour of the solution of equation 4 for case 1, $Pr = 1$

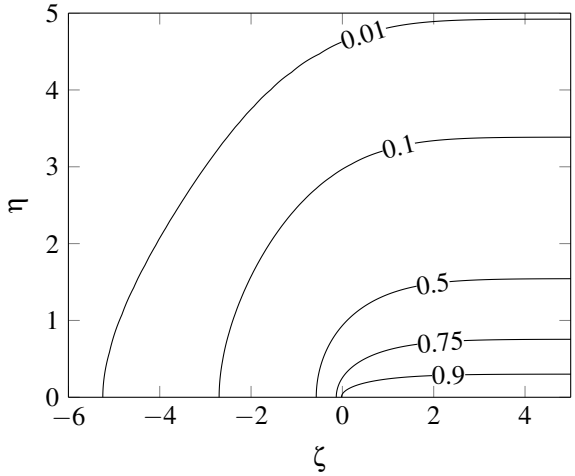

Figure 6. Nondimensional temperature (θ/θ_s) contour of the solution of equation 4 for case 2, $Pr = 1$

As shown in figure 9 through figure 12, the extension of the analogous conduction solution to the three dimensional domain by equating the height of the domain to the streamwise conduction thickness works remarkably well. While it might seem the

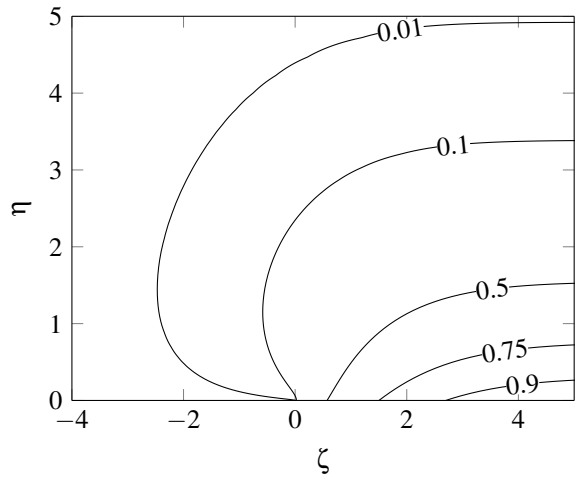

Figure 7. Nondimensional temperature ($k\theta/q''_s\Delta_c$) contour of the solution of equation 4 for case 3, $Pr = 1$

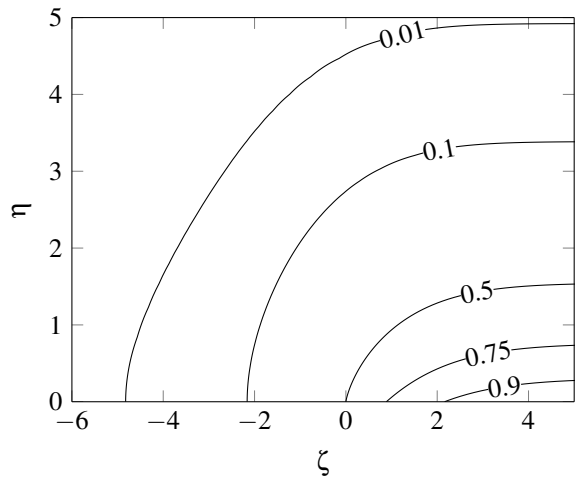

Figure 8. Nondimensional temperature ($k\theta/q''_s\Delta_c$) contour of the solution of equation 4 for case 4, $Pr = 1$

assumption of a constant conduction thickness in the lateral direction would cause difficulties, this turns out to not affect the solution near the edge of the plate. So while the conduction thickness does change near the edge of the plate, the local heat transfer is dominated by the nearby lateral discontinuity.

In cases 1–3 the conduction solution predicts an infinite heat transfer at the very edge of the plate. Cases 1, 2, and 3 show power law scaling as $\zeta^* \to 0$. This can easily be shown for case 1 by expanding $\exp(\pi\zeta^*)$ with a Taylor series in equation 18, and taking the limit for $\zeta^* \to 0$, which results in the scaling $Nu \propto 1/\zeta^*$. The power law behavior for cases 2 and 3 is not so easily extracted from equation 20 and equation 21, but figure 10 and figure 11 clearly indicate that a scaling of $Nu \propto {\zeta^*}^{-1/2}$. The scaling for case 2 is not unexpected, as Deegan, Bakajin, Dupont, Huber, Nagel, and Witten [9] reported the same power scaling for the analogous problem of diffusive evaporation droplet as the contact angle approaches 0.

The local *Nu* for the heated plate is shown in figure 9 through figure 12 for the two and three dimensional simulations. The points for the three dimensional case were taken at a specific x location so the graph was not cluttered, but the data collapses to the same curve for all x locations sufficiently far from the leading edge. The agreement with equation 18 through equation 22 is very good for every Pr, even with the introduction of an unheated starting length. Nevertheless the large increase of *Nu* at the edge will affect the average *Nu* on the heated plate, especially for small plates. Equation 18, equation 19, equation 20, equation 21, and equation 22 can therefore be a useful tool for modeling these problems.

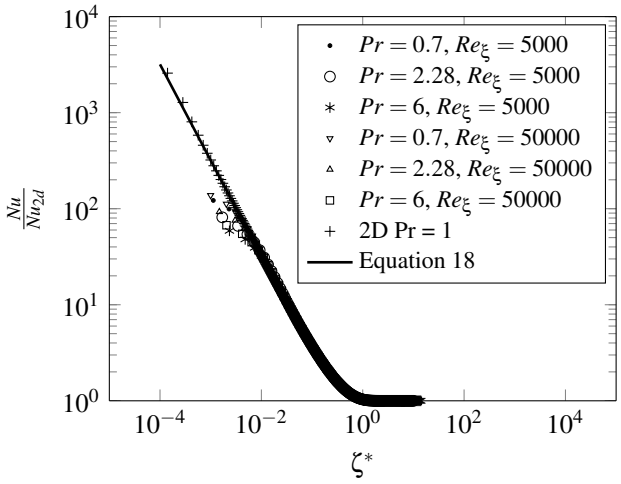

Figure 9. Comparison of numerical and analytical *Nu* for case 1

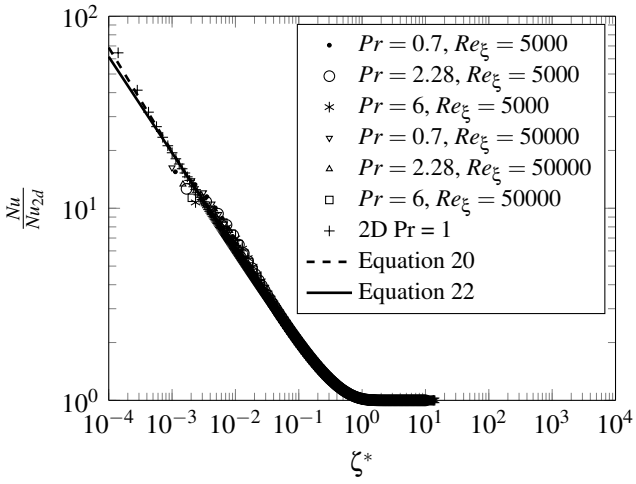

Figure 10. Comparison of numerical and analytical *Nu* for case 2

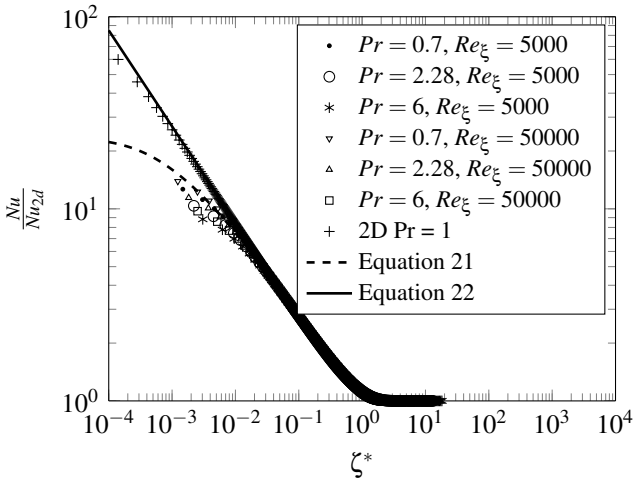

Figure 11. Comparison of numerical and analytical *Nu* for case 3

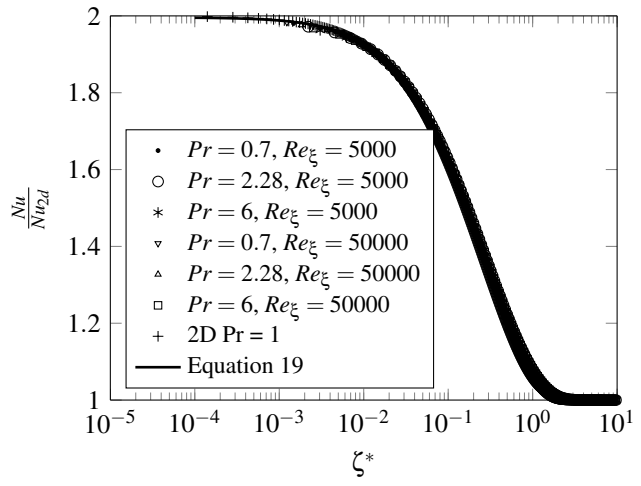

Figure 12. Comparison of numerical and analytical *Nu* for case 4

The convection correlations were shown to be fairly accurate in describing the *Nu* near the lateral edge of the heated plate. However, they should be used with caution near the leading and trailing edges of the plate, as the presented correlations will underestimate the local *Nu* due to large streamwise gradients. The numerical simulations showed that the expected two dimensional behavior was established very close to the leading edge ($Re_{x-\xi} > 50$), but more research is required to definitively say how close to the leading and trailing edges the proposed theory is valid. In addition, these correlations are only expected to be valid for the range of $Pr > 0.5$. If *Pr* is low, then streamwise conduction would become a important.

The correlation from Ortega [5] was constructed using a conduction solution for a moving heat source. Comparison with the proposed correlation, seen in figure 13, showed that Ortega [5] overestimated the extent of the edge effect by modeling assuming uniform flow and neglecting the boundary layer. As stated by Ortega [5], their correlation provides the large limiting case for the *Nu*. However, their model does offer a prediction of the thermal wake behind the heated surface, which is not addressed by the proposed model.

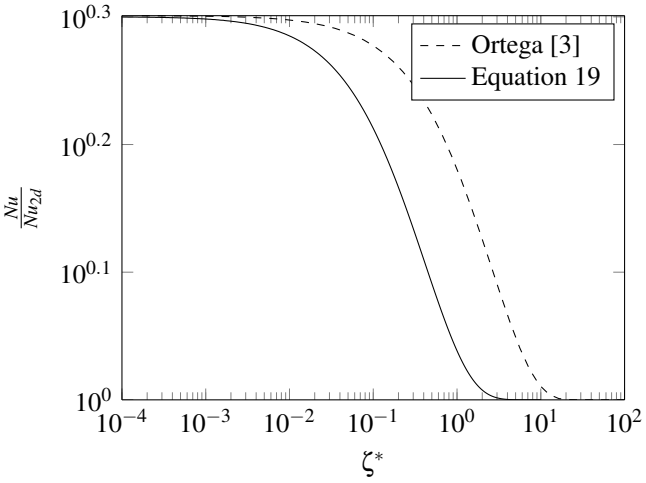

Figure 13. Comparison of equation 19 with [5]

CONCLUSIONS

Due to the limited transport in the laminar boundary layer, the conduction solution for analogous boundary conditions results a good correlation for *Nu* over the whole surface of a finite width flat plate. By extending the conduction solution to the laminar flow regime using the conduction thickness of the thermal boundary layer, *Nu* was shown to be a function of the nondimensional streamwise variables, ζ^*. The derived correlations compared well with numerical results from OpenFOAM without any parameter fitting. In practical applications the boundary conditions may not be well represented by the four cases studied here, but these results are useful limiting solutions. In general, the influence of the lateral discontinuity on the temperature and heat flux in the spanwise direction was comparable in length to the thermal boundary.

REFERENCES

[1] E. Baker, Liquid cooling of microelectronic devices by free and forced convection, Microelectronics and Reliability, 11, 1972, pp.213–222.

[2] S. Ramadhyani, D. F. Moffatt, F. P. Incropera, Conjugate heat transfer from small isothermal heat sources embedded in a large substrate, International Journal of Heat and Mass Transfer, 28, 1985, pp.1945–1952.

[3] A. Ortega, S. Ramanathan, On the use of point source solutions for forced air cooling of electronic components—Part 2: Conjugate forced convection from a discrete rectangular source on a thin conducting plate, Journal of Electronic Packaging, 125, 2003, pp.235–243.

[4] H. Bhowmik, Review on convection heat transfer in channel flow with discrete heater arrays for electronic cooling, International Journal of Engineering, Science and Technology, 6, 2014, pp.31–44.

[5] A. Ortega, S. Ramanathan, On the use of point source solutions for forced air cooling of electronic components—Part 1: Thermal wake models for rectangular heat sources, Journal of Electronic Packaging, 125, 2003, pp.226–234.

[6] M. M. Yovanovich, P. Teertstra, Laminar forced convection modeling of isothermal rectangular plates, Journal of Thermophysics and Heat Transfer, 15, 2001, pp.205–211.

[7] W. Kays, M. Crawford, B. Weigand, Convective heat and mass transfer, fourth edition, McGraw-Hill, 2004.

[8] E. G. Hauptmann, Z. Rotem, Spanwise thermal diffusion in low Prandtl number boundary layer flow, Proceedings of the Canadian Congress of Applied Mechanics, 2, 1967, pp.263–264.

[9] M. N. Ozisik, Heat conduction, second edition, Wiley, 1993.

[10] S. W. Churchill, R. Usagi, A general expression for the correlation of rates of transfer and other phenomena, AIChE Journal, 18, 1972, pp.1121–1128.

[11] R. D. Deegan, O. Bakajin, T. F. Dupont, G. Huber, S. R. Nagel, T. A. Witten, Capillary flow as the cause of ring stains from fired liquid drops, Nature, 389, 1997, pp.827–829.

NOMENCLATURE

Symbol	Quantity	SI Unit
A	Eigenfunction coefficient	–
B	Eigenfunction coefficent	–
c	Fitting parameter as $\zeta \to 0$	–
f	Solution to Blasius function, where $f'(\eta) = u/U_\infty$	–
h	Heat transfer coefficient (q''/θ_s)	$\mathrm{W\,m^{-2}\,K^{-1}}$
k	Thermal conductivity	$\mathrm{W\,m^{-1}\,K^{-1}}$
m	Fitting parameter	–
n	Positive integer	–
Nu	Nusselt number (hx/k)	–
Nu_{2d}	Nusselt number far from the edge	–
Pr	Prandtl number (ν/α)	–
q''_s	Wall heat flux	$\mathrm{W\,m^{-2}}$
Re_x	Reynolds number ($U_\infty x/\nu$)	–
T	Temperature	K
U	Velocity in x direction	$\mathrm{m\,s^{-1}}$
$\vec{V}$	Velocity vector	$\mathrm{m\,s^{-1}}$
u	x component of velocity	$\mathrm{m\,s^{-1}}$
v	y component of velocity	$\mathrm{m\,s^{-1}}$
w	z component of velocity	$\mathrm{m\,s^{-1}}$
x	Streamwise coordinate	m
y	Wall normal coordinate	m
z	Spanwise coordinate	m

Greek Symbol	Quantity	SI Unit
α	Thermal diffusivity	$\mathrm{m^2\,s^{-1}}$
Δ_c	Conduction thickness, x/Nu_{2d}	m
δ	Momentum boundary layer thickness	m
δ_T	Thermal boundary layer thickness	m
ζ	Spanwise variable, $z\sqrt{\frac{U_\infty}{\nu x}}$	–
ζ^*	Spanwise variable, $Nu_{2d}z/x$	–
η	Wall normal variable, $y\sqrt{\frac{U_\infty}{\nu x}}$	–
θ	Temperature difference ($T - T_\infty$)	K
λ	Eigenvalue	$\mathrm{m^{-1}}$
ν	Kinematic viscosity	$\mathrm{m^2\,s^{-1}}$
ξ	Unheated starting length	m

Subscript	Description
1	Domain above heated surface
2	Domain above cold surface
F	Flux specified boundary condition
s	Evaluated at the surface
T	Temperature specified boundary condition
∞	Freestream